AGU PUBLICATIONS

Geophysical Research Letters

RESEARCH LETTER
10.1002/2017GL073681

Key Points:
- We estimate a proxy for slip-weakening distance D_c'' from near-fault record of the 2016 *M*7.8 Kaikōura (New Zealand) earthquake
- The D_c'' is 4.9 m at station KEKS, the largest value ever estimated from near-fault strong motion data
- The large D_c'' appears to follow the scaling D_c'' with final slip for several large strike-slip earthquakes

Correspondence to:
Y. Kaneko,
y.kaneko@gns.cri.nz

Citation:
Kaneko, Y., E. Fukuyama, and I. J. Hamling (2017), Slip-weakening distance and energy budget inferred from near-fault ground deformation during the 2016 M_w7.8 Kaikōura earthquake, *Geophys. Res. Lett.*, *44*, doi:10.1002/2017GL073681.

Received 31 MAR 2017
Accepted 30 APR 2017
Accepted article online 3 MAY 2017

Slip-weakening distance and energy budget inferred from near-fault ground deformation during the 2016 M_w7.8 Kaikōura earthquake

Yoshihiro Kaneko[1], **Eiichi Fukuyama**[2], **and Ian James Hamling**[1]

[1]GNS Science, Lower Hutt, New Zealand, [2]National Research Institute for Earth Science and Disaster Resilience, Tsukuba, Japan

Abstract The 2016 *M*7.8 Kaikōura (New Zealand) earthquake struck the east coast of the northern South Island, resulting in strong ground shaking and large surface fault slip. Since the earthquake was well recorded by a local strong-motion seismic network, near-fault data may provide direct measurements of dynamic parameters associated with the fault-weakening process. Here we estimate a proxy for slip-weakening distance D_c'', defined as double the fault-parallel displacement at the time of peak ground velocity, from accelerograms recorded at a near-fault station. Three-component ground displacements were recovered from the double numerical integration of accelerograms, and the corresponding final displacements are validated against coseismic displacement from geodetic data. The estimated D_c'' is 4.9 m at seismic station KEKS located ~2.7 km from a segment of the Kekerengu fault where large surface fault slip (~12 m) has been observed. The inferred D_c'' is the largest value ever estimated from near-fault strong motion data, yet it appears to follow the scaling of D_c'' with final slip for several large strike-slip earthquakes. The energy budget of the *M*7.8 Kaikōura earthquake inferred from the scaling of D_c'' with final slip indicates that a large amount of energy was dissipated by on- and off-fault inelastic deformation during the propagation of the earthquake rupture, resulting in a slower average rupture speed ($\lesssim$2.0 km/s).

Plain Language Summary Slip-weakening distance is a parameter controlling the evolution of fault slip during an earthquake and is important for understanding rupture dynamics. However, it has been debated how large slip-weakening distance is and whether it scales with fault slip. We present evidence for large slip-weakening distance estimated from near-fault record of the recent magnitude 7.8 Kaikōura (New Zealand) earthquake. By examining seismic waveforms of the Kaikōura quake, we find that the slip-weakening distance is about 5 m on a portion of the Kekerengu fault, the largest value ever estimated directly from near-fault records. The large slip-weakening distance implies that a large amount of energy was dissipated by on- and off-fault inelastic deformation during the propagation of earthquake rupture, which may explain why the rupture propagation velocity of the Kaikōura quake was slower than that of most crustal earthquakes.

1. Introduction

Fault weakening during the propagation of seismic rupture is a key process governing the earthquake rupture dynamics and energy partitioning. One of the important parameters for characterizing a fault-weakening process is the slip-weakening distance D_c. In the framework of slip-weakening friction [*Ida*, 1972; *Palmer and Rice*, 1973], the frictional strength of a fault decreases from the peak to residual level (referred to as breakdown strength drop) over slip-weakening distance D_c (Figure 1a). The corresponding fracture energy, which is the work done on the fault surface (the green area in Figure 1a), can be calculated by integrating the shear stress up to D_c [*Tinti et al.*, 2005a]. Although slip-weakening distance has been measured in laboratory analogue experiments [e.g., *Ohnaka et al.*, 1987; *Ohnaka*, 2003], how large D_c is and whether it scales with the amount of coseismic slip are not well understood for real earthquakes.

Slip-weakening distance D_c for large earthquakes can be inferred from inversion of seismic waveforms for the source parameters [e.g., *Ide and Takeo*, 1997; *Pulido and Irikura*, 2000; *Tinti et al.*, 2005a; *Ruiz and Madariaga*, 2011; *Causse et al.*, 2014; *Twardzik et al.*, 2014]. Based on kinematic inversion of fault slip for the 1995 *M*6.9 Kobe (Japan) earthquake, *Ide and Takeo* [1997] estimated D_c from the spatiotemporal stress evolution on the

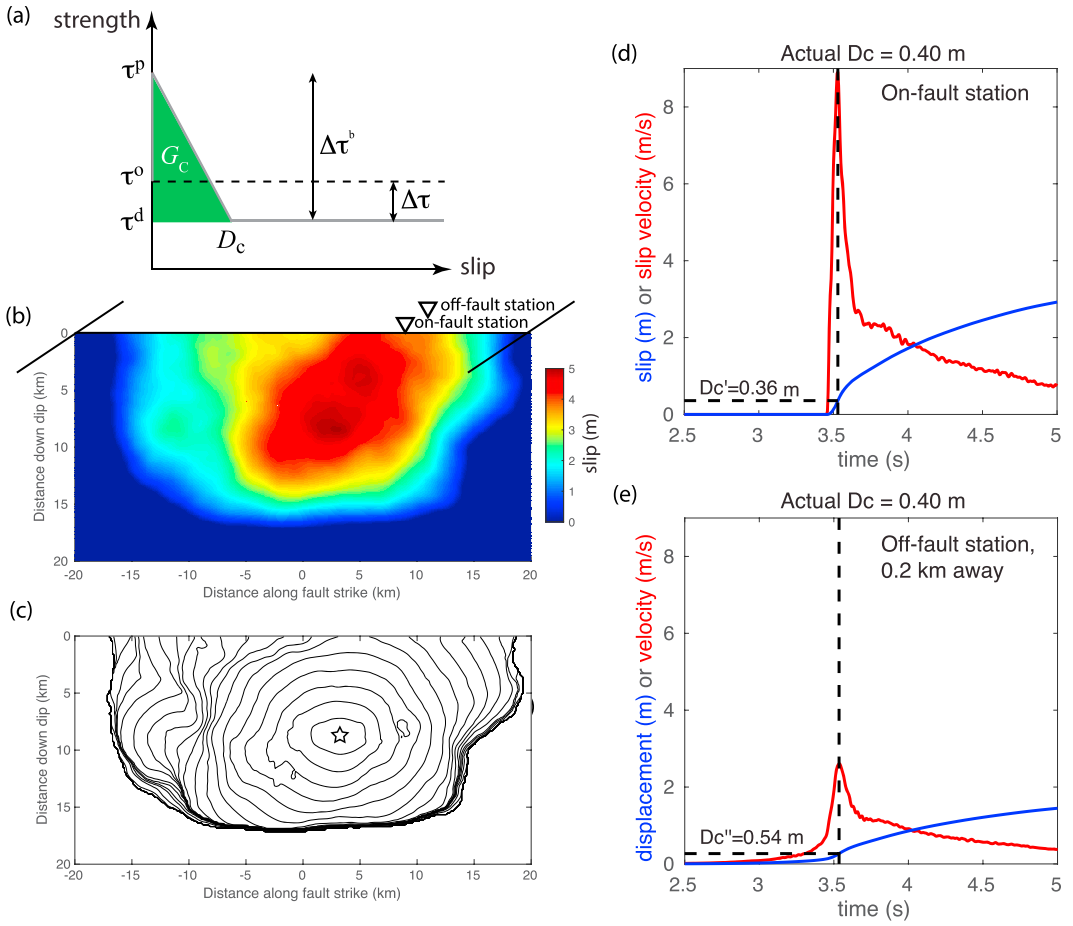

Figure 1. (a) Linear slip-weakening friction law. The shear strength linearly decreases from its static strength τ^p to the dynamic value τ^d over the characteristic fault slip distance D_c. The initial shear stress τ^o, fracture energy G_c, static stress drop $\Delta\tau$, and breakdown strength drop $\Delta\tau^b$ are also indicated. (b) Slip distribution of a synthetic earthquake considered by Problem TPV16 of the SCEC/USGS dynamic rupture code verification exercise [*Harris et al.*, 2009]. The numerical solution of Kaneko based on the spectral element method [*Kaneko et al.*, 2008] is shown. Inverted triangles show on-fault and off-fault (0.2 km away) station locations. An assumed heterogeneous prestress distribution on the fault results in a heterogeneous fault slip distribution. The contours are plotted every 0.5 s. Star indicates the hypocenter. (d) Evolution of slip and slip velocity at the on-fault station. (e) Displacement and particle velocity waveforms at the off-fault station 0.2 km away from the fault. The technique developed by *Mikumo et al.* [2003] and *Fukuyama and Mikumo* [2007] yields $D_c' = 0.36$ m and $D_c'' = 0.54$ m, which differ from the actual D_c by 10% and 35%, respectively.

fault. More recently, *Twardzik et al.* [2014] applied dynamic inversion and inferred fault-weakening parameters including D_c from the waveforms of the 2004 *M*6.0 Parkfield (California) earthquake. However, it is generally difficult to reliably constrain D_c from inversion of seismic waveforms due to the usage of band-limited seismic data [*Guatteri and Spudich*, 2000] or various trade-offs among dynamic parameters during the spatiotemporal evolution of fault slip [*Cocco et al.*, 2009; *Goto and Sawada*, 2010].

Mikumo et al. [2003] and *Fukuyama and Mikumo* [2007] proposed a method for estimating D_c directly from displacement and velocity waveforms recorded at a near-fault seismic station. This method is illustrated in Figure 1, with the application to a synthetic strike-slip earthquake considered by the Southern California Earthquake Center (SCEC)/U.S. Geological Survey (USGS) dynamic rupture code verification exercise [*Harris et al.*, 2009, 2011]. In the case of a vertical strike-slip fault, numerical models show that D_c' defined as the amount of fault-parallel slip at the time of the peak fault-parallel slip velocity, approximately coincides with the actual D_c on the fault (Figure 1d). In reality, seismic stations are not located exactly on the ruptured fault, in which case, off-fault version D_c'', defined as double the fault-parallel ground displacement at the time of the peak fault-parallel velocity, can be used to roughly estimate D_c on the fault (Figure 1e). The method works reasonably well even for the case of a heterogeneous prestress distribution on a fault, which results in

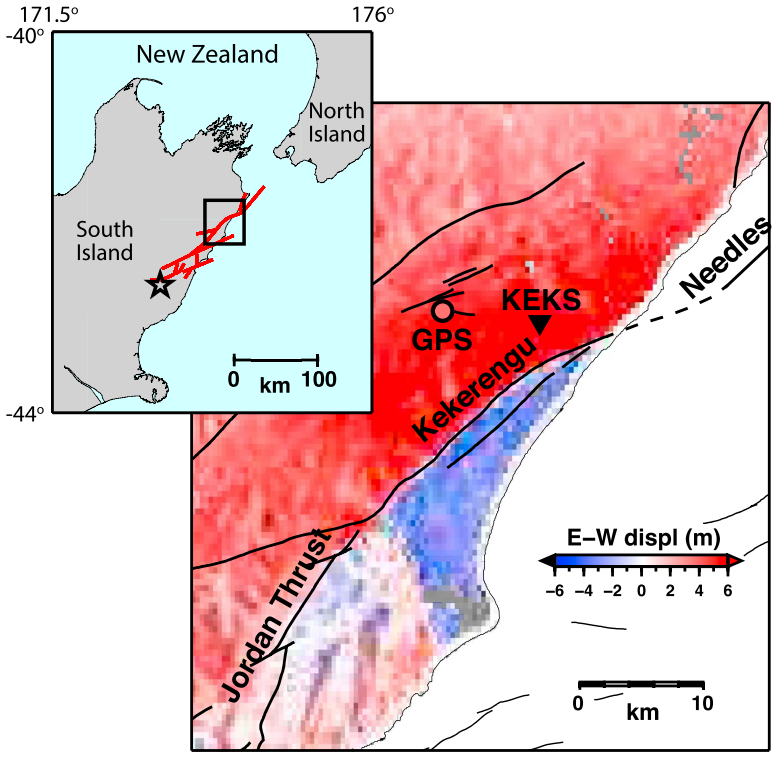

Figure 2. East-west horizontal displacement field derived from Sentinel-1A ascending (3–15 November 2016) and descending (5 September to 16 November 2016) azimuth and range offsets [*Hamling et al.*, 2017]. Black lines show the location of mapped active faults [*Langridge et al.*, 2016]. Inverted triangle is the location of strong-motion station KEKS. The circle indicates equivalent displacement at a campaign GPS site with the measurement made a few days after the *M*7.8 Kaikōura earthquake. Inset map shows the surface traces of ruptured faults (red lines) [*Hamling et al.*, 2017] and the epicenter of the *M*7.8 Kaikōura earthquake (black star).

nonuniform slip and rupture speeds (Figures 1b and 1c). The assumed D_c is spatially uniform on the fault in this example (Figure 1), whereas a heterogeneous distribution of D_c likely introduces additional uncertainty in the resulting D_c estimate. For dip-slip faulting, the magnitudes of foot wall and hanging wall displacements are not usually equal, and hence, near-fault records on both sides of the fault are needed to estimate D_c''.

The above mentioned method has been applied to several large strike-slip earthquakes where near-fault waveform records were available. For example, *Fukuyama and Suzuki* [2016] used waveforms recorded at station KMMH16 located ~500 m from a fault ruptured during the 2016 *M*7.1 Kumamoto (Japan) earthquake and obtained D_c'' = 1.1 m. In the case of the 2002 *M*7.9 Denali (Alaska) earthquake, D_c'' was estimated to be ~2.5 m at seismic station PS10 located about 3 km away from the fault [*Fukuyama and Mikumo*, 2007]. Since these seismic stations are not located on the fault, one needs to consider the resolution distance over which estimated D_c'' is still related to the actual D_c on the fault. *Cruz-Atienza et al.* [2009] investigated the accuracy of D_c'' estimates using numerical simulations of strike-slip earthquakes and concluded that for this method to work reasonably well, the seismic station must be located within the resolution distance R_c from the fault, where R_c is given by 0.8 times the wavelength at a breakdown frequency, defined as the reciprocal of the time over which the stress decreases to the dynamic level. Recently, *Galetzka et al.* [2015] applied a similar method relating the shape of a slip-rate time function to the characteristics of a friction law [*Tinti et al.*, 2005b] and estimated D_c of ~5 m from waveforms at stations located ~10 km from a fault ruptured during the *M*7.8 Gorkha (Nepal) earthquake. However, relatively large fracture energy associated with the large D_c (which was estimated only from the hanging wall seismic-station records) together with the peak slip of 6.5 m may not be compatible with the fast rupture speed of ~3.3 km/s inferred for this earthquake.

The 13 November 2016 *M*7.8 Kaikōura earthquake in the northern South Island of New Zealand was well recorded by a local network of strong motion sensors, providing an opportunity to estimate slip-weakening distance from near-fault seismograms. Among those strong-motion sensors, station KEKS (latitude −41.95569°,

longitude 173.98141°, and elevation 339 m) is located ~2.7 km away from the surface trace of the Kekerengu fault (Figure 2) where large (~12 m) dextral surface slip has been imaged by SAR (synthetic aperture radar) data and identified by field observations [*Hamling et al.*, 2017]. The station is equipped with Kinemetrics FBA-ES-T force balance accelerometer (http://www.kinemetrics.com/p-87-EpiSensor-ES-T.aspx). A fault slip model derived from the inversion of SAR, GPS, and field measurements suggests that the earthquake rupture was complex involving at least 12 major fault segments with multiple focal mechanisms, extending over ~180 km from northern Canterbury to Cook Strait (Figure 2) [*Hamling et al.*, 2017]. Despite the complexity, the main asperity (i.e., an area of large fault slip) with slip of up to ~25 m appears to be concentrated on a single, continuous fault network spanning across the Jordan Thrust, Kekerengu, and Needles faults, with predominately strike-slip motion in the upper ~10 km of the Kekerengu fault [*Hamling et al.*, 2017]. Hence, the near-fault seismic record may provide the first direct estimate of slip-weakening distance on a fault segment with a significant (>10 m) amount of coseismic slip.

In this study, we examine near-fault seismograms at station KEKS close to the Kekerengu fault and estimate slip-weakening parameter D_c'' using the above mentioned method. We discuss the scaling of D_c'' with the final slip, the corresponding fault-weakening parameters, and earthquake energy partitioning for the *M*7.8 Kaikōura quake.

2. Method

The accelerograms recorded at station KEKS were used to obtain ground displacement as follows: We first corrected for the instrument response by multiplying the unfiltered acceleration by a constant value and converted the digits to a physical measure (i.e., m/s^2). To set the beginning of the waveform to zero, a constant value is subtracted from each acceleration waveform. Next, the horizontal components of the acceleration seismic record were rotated into fault-parallel (N241°) and fault-normal (N331°) components using the fault strike at the closest point on the Kekerengu fault trace from station KEKS (Figure 2). We then numerically integrated the acceleration waveforms in time and obtained velocity waveforms.

Figure 3 shows the three-component seismic velocity waveforms at station KEKS. While the vertical component of the velocity waveform is reasonable, baseline drift can be seen in the horizontal components. Baseline drift is commonly observed in waveforms recorded by near-field strong motion sensors, and the origin can be attributed to either instrumental noise, often caused by the friction of spring in the sensor, or natural distortions of ground likely due to tilting [e.g., *Boore*, 2001; *Graizer*, 2010; *Van Houtte et al.*, 2017]. Since the signal-to-noise ratio is high and station KEKS is at a "hard rock" site with $V_{s\,30}$~1000 m/s [*Kaiser et al.*, 2017a], the distortion of the waveforms likely originated from ground tilt rather than instrumental noise. After careful visual inspection of these waveforms, we assumed that the baseline drift was caused by ground tilt that occurred at $t = 64$ s after the origin time (Figure 3). To correct for the baseline drift, a linear trend (a purple line in Figure 3), defined between the tilt start time and a quiet portion of the velocity trace sometime after the strong shaking, was removed from the horizontal components of the velocity waveforms. We then numerically integrated the velocity waveforms in time and obtained displacement waveforms (Figure 3).

As discussed in *Graizer* [2010], correcting for baseline drift is not a unique process especially when the cause is not known and there is no other data (e.g., ground rotation) at the same site. To validate the double-integrated displacements shown in Figure 3, we compare the final displacements to coseismic displacements derived from SAR azimuth and range offsets at the location of station KEKS and the closest (~7 km away) campaign GPS site (Figure 2). We find that the final vertical and east-west displacements agree well with those estimated by SAR and GPS data (error $\lesssim$3%), whereas there is a larger difference in the north-south displacement for the SAR data (error ~50%). SAR data are not generally sensitive to north-south ground deformation as it coincides with the direction of moving satellites. Nevertheless, the fault-parallel component, which is used to estimate slip-weakening distance, agrees reasonably well with the SAR and closest GPS data (errors $\lesssim$12%) (Figure 3). Note that we did not correct for the frequency response of the strong-motion sensor. Since the acceleration response at low frequency is flat and our focus is the near-fault displacement, the uncorrected high-frequency response does not affect the present analysis.

In addition to station KEKS, waveforms at other near-fault seismic and high-rate GPS stations were also examined. However, these stations are either located more than 10 km away from the closest rupture fault or the closest fault had dominant dip-slip motion inferred from a fault slip model [*Hamling et al.*, 2017], and hence, they are not discussed in this study.

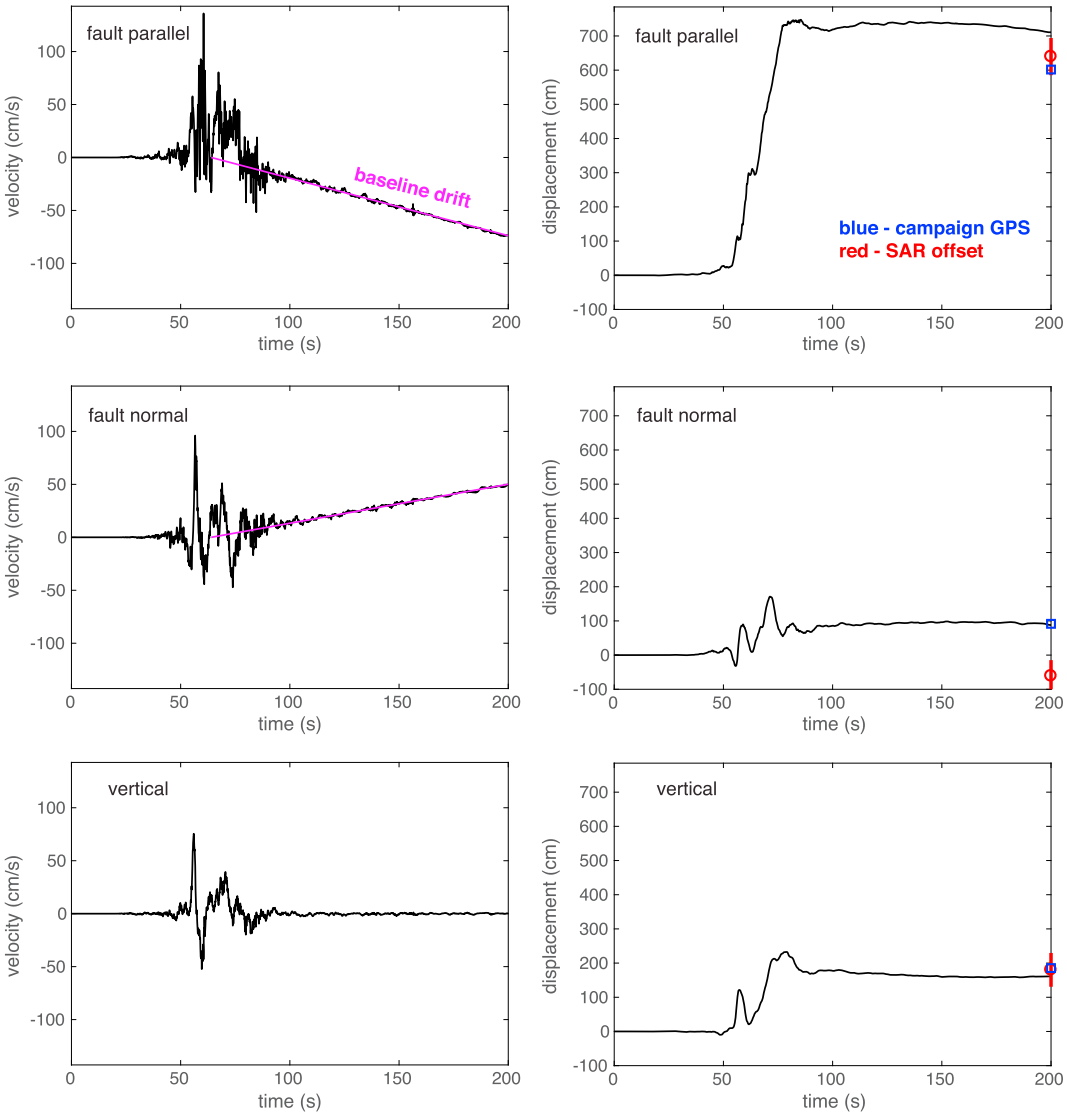

Figure 3. Three-component, unfiltered seismic velocity, and displacement waveforms at station KEKS recovered from the acceleration waveforms. The time (t = 0) corresponds to the origin time of the M7.8 Kaikōura earthquake. Blue square and red circle indicate coseismic displacement measured at a nearby campaign GPS site and estimated from SAR (synthetic aperture radar) azimuth and range offset at the location of KEKS, respectively (Figure 2). The vertical red line shows the error associated with the azimuth and range offsets.

3. Estimated D_c'' and Its Scaling With Final Slip

Following the method of *Mikumo et al.* [2003] and *Fukuyama and Mikumo* [2007], we measure the amount of fault-parallel displacement at the time of the peak ground velocity, which is multiplied by the factor of 2 to obtain D_c'' (Figure 4a). The estimated D_c'' is 4.9 m at station KEKS, which is quite large compared to previous estimates of D_c'' for other earthquakes. To assess the accuracy of the estimated D_c'', we calculate the resolution distance given by $R_c = 0.8V_sT_c$, where V_s is the shear wave velocity and T_c is the breakdown time [*Cruz-Atienza et al.*, 2009]. We assume that $V_s = 2390$ m/s derived from the spatial average of V_s in the upper 2 km of the local 3-D velocity model obtained by body wave tomography [*Eberhart-Phillips et al.*, 2010]. The breakdown time $T_c = 5.5$ s, which corresponds to a duration over which the displacement began to increase rapidly until the time of the peak ground velocity (Figure 4a). This means that $R_c = 0.8V_sT_c = 10.5$ km at station KEKS, which is much larger than the distance from the station to the surface trace of the fault (~2.7 km). Hence, the seismic station was located within the resolution distance, and the estimated D_c'' may represent the actual slip-weakening distance D_c averaged over the upper few kilometers of the Kekerengu fault. As found

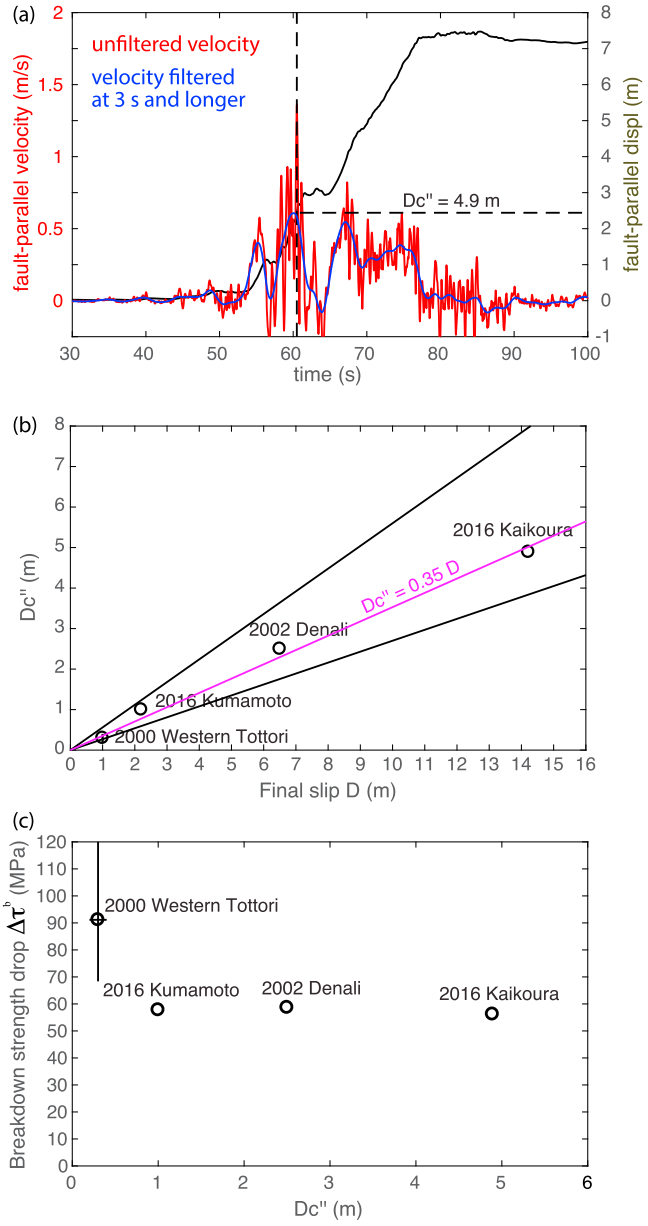

Figure 4. (a) Fault-parallel displacement and velocity waveforms at KEKS. Both unfiltered (red) and filtered (blue) velocity waveforms are shown. Dashed lines show the time of the peak (unfiltered) velocity and the corresponding displacement, respectively. (b) Comparison between D_c'' and the final slip D estimated from near-fault ground-deformation records during four large earthquakes. A purple line ($D_c = 0.35D$) shows a least squares fit to the data points. Two solid black lines are the upper and lower limits of D_c ($D_c'' = 0.56D$ and $D_c'' = 0.27D$) estimated by *Mikumo et al.* [2003]. (c) The corresponding breakdown strength drop, $\Delta\tau^b = \tau^p - \tau^d$, assuming that the estimated D_c'' are equal to D_c and the scaling of fracture energy with slip [*Viesca and Garagash*, 2015] holds in these cases.

in *Mikumo et al.* [2003] and *Fukuyama and Mikumo* [2007], the actual slip-weakening distance D_c and estimated D_c'' can differ by up to 50% due to inaccuracy introduced by the method. Hence, our result indicates that $D_c = 4.9 \pm 2.4$ m on the fault.

Unlike the synthetic example shown in Figure 1e, the fault-parallel velocity waveform is complex, with multiple peaks (Figure 4a). To understand the origin of the complex waveform and its effect on the D_c'' estimate, we low-pass filtered the waveform at the period of 3 s and longer (a blue curve in Figure 4a). The time of the peak filtered velocity is nearly identical to that of the unfiltered velocity, and hence, the D_c'' estimate was not affected by the frequency down to 0.333 Hz. We interpret the first, smaller peak at $t = 55.5$ s to be shear wave arrival at station KEKS due to the rupturing of fault segments closer to the epicenter of the Kaikōura earthquake (Figure 4a). The second, larger peak at $t = 60.5$ s would correspond to the rupturing of the Kekerengu fault segment near station KEKS (Figure 4a). Interestingly, the third, smaller peak at $t = 67$ s and subsequent motion resulted in large dynamic deformation (Figure 4a), indicating that the Kekerengu fault may have ruptured twice in the short time interval ($\lesssim$20 s).

The estimated D_c'' at KEKS station is the largest value ever estimated from near-fault strong motion data. The largest D_c'' previously estimated was for the 2002 *M*7.9 Denali (Alaska) earthquake at station PS10 ($D_c'' = 2.5$ m). Interestingly, the estimated D_c'' for the Kaikōura earthquake appears to follow the scaling of D_c'' with final slip (Figure 4b) inferred from previous studies [*Fukuyama and Mikumo*, 2007; *Fukuyama and Suzuki*, 2016]. For the final slip D of the Kaikōura earthquake, we take double the final fault-parallel displacement ($D = 14$ m), which agrees fairly well with the dextral surface offset (12 m) reported from SAR offset and field observations [*Hamling et al.*, 2017]. A least squares fit of a line to data points shown Figure 4b gives $D_c'' = 0.35D$. This apparent scaling of D_c'' with the final slip indicates that the slip-weakening distance D_c is 30–50% of the final slip, as suggested by *Mikumo et al.* [2003] (two solid lines in Figure 4b). The inferred scaling is also consistent with observational studies indicating that earthquake fracture energy increases with the amount of fault slip [*Abercrombie and Rice*, 2005; *Viesca and Garagash*, 2015].

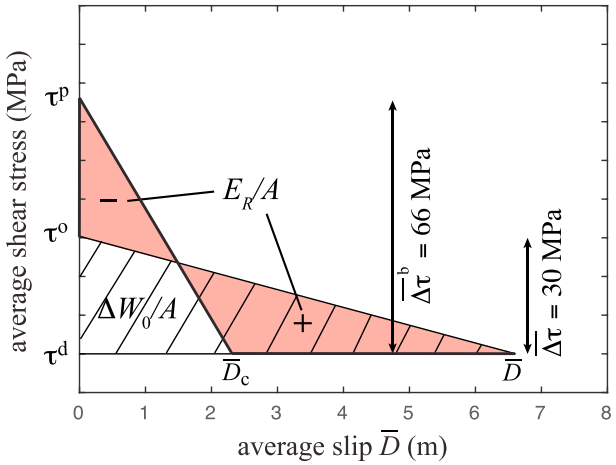

Figure 5. Energy partitioning during the *M*7.8 Kaikōura earthquake inferred from estimated fault-weakening parameters. Estimated parameters including spatial averages of slip $\overline{D}$, slip-weakening distance $\overline{D_c}$, static stress drop $\overline{\Delta\tau}$, and breakdown strength drop $\overline{\Delta\tau^b}$ are indicated. The striped region corresponds to available energy over the ruptured fault area $\Delta W_0/A$. A large portion of available energy may have been dissipated as fracture energy, resulting in low radiation efficiency ($\eta_{\text{eff}} = 0.24$) and slow earthquake rupture speed ($\lesssim$2.0 km/s).

4. Breakdown Strength Drop and Energy Budget

The scaling of fracture energy with slip [*Abercrombie and Rice*, 2005; *Viesca and Garagash*, 2015] can provide a constraint on the range of D_c expected from the final slip of 14 m on the Kekerengu fault. Assuming that the scaling of fracture energy with slip over many orders of magnitude of earthquake sizes (a black curve in Figure 3 of *Viesca and Garagash* [2015]) holds and that the fault weakening is governed by linear slip-weakening friction with $D_c = 4.9$ m, the corresponding fracture energy $G_c = 1.4 \times 10^8$ J/m^2, which leads to the breakdown strength drop $\Delta\tau^b = 2G_c/D_c = 56$ MPa. Note that qualitatively similar scaling laws for fracture energy versus slip over a smaller slip range (up to 6.5 m) were developed by other investigators [*Causse et al.*, 2014; *Nielsen et al.*, 2016; *Cocco et al.*, 2016]; here we use the scaling law described in *Viesca and Garagash* [2015] that extends slip of up to ~20 m.

To assess the feasibility of the inferred breakdown strength drop, we calculate static stress drop for the largest asperity close to station KEKS that spans across the Jordan Thrust, Kekerengu, and Needles fault segments in the fault slip model of *Hamling et al.* [2017]. The shear stress changes were obtained assuming the point-source dislocation solution of *Okada* [1992] in an elastic half-space. From the definition of so-called energy-based stress drop [*Noda et al.*, 2013], we obtain $\Delta\tau = 36$ MPa for the asperity, which is 64% of the inferred strength drop. The relatively large strength drop of 56 MPa is reasonable because the static stress drop is also large compared to those associated with the asperities of other large crustal earthquakes ($\Delta\tau \sim 10$ MPa) [*Irikura and Miyake*, 2011]. If the actual slip-weakening distance were much smaller, for example, $D_c = 1.0$ m, then $\Delta\tau^b$ would be 300 MPa, much larger than the lithostatic normal stress in the upper 5 km which is unrealistic.

Applying the similar analysis to other earthquakes with previously estimated D_c'' and D (Figure 4b), we infer the corresponding breakdown strength drop $\Delta\tau^b$. Remarkably, $\Delta\tau^b$ is relatively stable among events with different final slip and in the range of 56–60 MPa except for the 2000 *M*6.6 Western Tottori (Japan) earthquake that led to a large uncertainty in $\Delta\tau^b$ (Figure 4c). The deviation of $\Delta\tau^b$ for the the 2000 *M*6.6 Western Tottori (Japan) earthquake may be attributed to difficulty in inferring the D_c from D_c'' with this method [*Cruz-Atienza et al.*, 2009]. Figure 4c indicates that while D_c may be scale dependent, the breakdown strength drop is independent of the final slip and slip-weakening distance, as proposed by the laboratory study of *Ohnaka and Shen* [1999]. In addition, relatively large strength drop implies that the stress drop is nearly complete and the residual shear stress is near zero for these events. Note that the assumed scaling of fracture energy versus slip [*Abercrombie and Rice*, 2005; *Viesca and Garagash*, 2015] was derived from an average estimate of all the faults ruptured during an earthquake, which can be quite different from punctual (or local) estimates [*Cocco et al.*, 2016] and lead to some uncertainty in the estimates of $\Delta\tau^b$ shown in Figure 4c.

To further examine the implication of the large slip-weakening distance and the scaling of D_c'' with slip D, we consider an energy partitioning diagram of the Kaikōura earthquake, assuming that (i) the scaling $D_c'' = 0.35D$ (Figure 4b) applies to all the fault segments ruptured during the earthquake, (ii) slip-weakening distance D_c on individual faults are equal to D_c'' (i.e., there is a distribution of D_c), and (iii) the scaling of fracture energy with slip [*Abercrombie and Rice*, 2005; *Viesca and Garagash*, 2015] holds for individual fault segments. During an earthquake, the stored elastic strain energy is partitioned into radiated energy, fracture energy, and heat [*Kostrov*, 1974]. The radiation efficiency η_{eff}, defined as the ratio of the radiated energy E_R to energy available

for seismic wave radiation and dissipation ΔW_0, is given by $\eta_{\text{eff}} = E_R/\Delta W_0$, where $\Delta W_0 = (1/2)\Delta\tau\overline{D}A$, $\Delta\tau$ is the static stress drop, and $\overline{D}$ is the average slip over the rupture area A [*Kanamori and Heaton*, 2000; *Rivera and Kanamori*, 2005]. Based on the slip distribution of *Hamling et al.* [2017] with the subduction interface, we calculate average slip $\overline{D}=6.6$ m, average slip-weakening distance $\overline{D_c}=0.35\overline{D}=2.3$ m, average static stress drop $\overline{\Delta\tau}=30$ MPa, and average breakdown strength drop $\overline{\Delta\tau^b}=2\overline{G_c}/\overline{D_c}=66$ MPa on all the fault patches with slip >10% of the maximum slip. Then the radiation efficiency of the Kaikōura earthquake can be calculated from an energy partitioning diagram constructed from estimated fault-weakening parameters (Figure 5). The available energy ΔW_0 (the striped triangle in Figure 5) is smaller than the radiated energy E_R given by the difference between the red areas marked by "plus" and "minus." From the diagram, the corresponding radiation efficiency $\eta_{\text{eff}} = 0.24$, which is given by the ratio of E_R to ΔW_0. The relatively small η_{eff} implies that the average rupture speed of the Kaikōura earthquake was slower than that of most crustal earthquakes ($\gtrsim$2.5 km/s) [*Heaton*, 1990; *Ye et al.*, 2016]. Preliminary finite-fault source inversion for the Kaikōura earthquake [*Kaiser et al.*, 2017b] indicates that the average rupture speed was $\lesssim$2.0 km/s, which is consistent with the inferred small radiation efficiency. The slow average rupture speed can be attributed to the fact that the Kaikōura earthquake broke relatively young and immature faults [*Wood et al.*, 1994; *Yeats and Berryman*, 1987], the process in which the large amount of available energy may have been dissipated by on- and off-fault inelastic deformation.

5. Conclusions

Using near-fault seismic velocity and displacement waveforms associated with the 2016 *M*7.8 Kaikōura earthquake, we find that a proxy for the slip-weakening distance, $D_c'' = 4.9$ m at station KEKS, which is located ~2.7 km away from the Kekerengu fault. This slip-weakening distance D_c'' is the largest value ever estimated from near-fault seismic records. Our analysis of these waveforms concludes that station KEKS is located within the resolution distance, suggesting that D_c'' may represent the actual slip-weakening distance D_c on the Kekerengu fault.

Our results further show that the estimated D_c'' appears to follow the scaling of D_c'' with final slip for large strike-slip earthquakes, while inferred breakdown strength drop remains roughly independent of D_c'' and final slip. In addition, energy partitioning associated with the large slip-weakening distance indicates small radiation efficiency ($\eta_{\text{eff}} = 0.24$) of the Kaikōura earthquake, consistent with a relatively slow average rupture speed ($\lesssim$2.0 km/s). This implies that a large amount of energy was dissipated by on- and off-fault inelastic deformation during the propagation of the earthquake rupture. Inferred fault-weakening parameters including slip-weakening distance and strength drop may be validated with well-calibrated dynamic rupture simulations.

Acknowledgments
We thank Laura Wallace, Nadia Lapusta, Ralph Archuleta, Chris Van Houtte, and Jean-Philippe Avouac for helpful discussions, and Robert Viesca for providing us the published scaling relation for fracture energy versus slip. We also thank Ruth Harris and an anonymous reviewer for their comments that helped us improve the manuscript. Y.K. and I.J.H. were supported by public funding from the Government of New Zealand. The strong-motion data used in this study are available to public and can be downloaded from New Zealand's GeoNet (https://www.geonet.org.nz).

References

Abercrombie, R. E., and J. R. Rice (2005), Can observations of earthquake scaling constrain slip weakening?, *Geophys. J. Int.*, *162*(2), 406–424, doi:10.1111/j.1365-246x.2005.02579.x.

Boore, D. M. (2001), Effect of baseline corrections on displacements and response spectra for several recordings of the 1999 Chi-Chi, Taiwan, earthquake, *Bull. Seismol. Soc. Am.*, *91*(5), 1199–1211.

Causse, M., L. A. Dalguer, and P. M. Mai (2014), Variability of dynamic source parameters inferred from kinematic models of past earthquakes, *Geophys. J. Int.*, *196*, 1754–1769, doi:10.1093/gji/ggt478.

Cocco, M., E. Tinti, C. Marone, and A. Piatanesi (2009), Scaling of slip weakening distance with final slip during dynamic earthquake rupture, *Int. Geophys.*, *94*, 163–186, doi:10.1016/S0074-6142(08)00007-7.

Cocco, M., E. Tinti, and A. Cirella (2016), On the scale dependence of earthquake stress drop, *J. Seismolog.*, *20*(4), 1151–1170, doi:10.1007/s10950-016-9594-4.

Cruz-Atienza, V. M., K. B. Olsen, and L. A. Dalguer (2009), Estimation of the breakdown slip from strong-motion seismograms: Insights from numerical experiments, *Bull. Seismol. Soc. Am.*, *99*(6), 3454–3469.

Eberhart-Phillips, D., M. Reyners, S. Bannister, M. Chadwick, and S. Ellis (2010), Establishing a versatile 3-D seismic velocity model for New Zealand, *Seismol. Res. Lett.*, *81*(6), 992–1000.

Fukuyama, E., and T. Mikumo (2007), Slip-weakening distance estimated at near-fault stations, *Geophys. Res. Lett.*, *34*, L09302, doi:10.1029/2006GL029203.

Fukuyama, E., and W. Suzuki (2016), Near-fault deformation and Dc'' during the 2016 M_w7.1 Kumamoto earthquake, *Earth Planets Space*, *68*(1), 194, doi:10.1186/s40623-016-0570-6.

Galetzka, J., et al. (2015), Slip pulse and resonance of the Kathmandu basin during the 2015 Gorkha earthquake, Nepal, *Science*, *349*(6252), 1091–1095.

Goto, H., and S. Sawada (2010), Trade-offs among dynamic parameters inferred from results of dynamic source inversion, *Bull. Seismol. Soc. Am.*, *100*(3), 910–922, doi:10.1785/0120080250.

Graizer, V. (2010), Strong motion recordings and residual displacements: What are we actually recording in strong motion seismology?, *Seismol. Res. Lett.*, *81*(4), 635–639.

Guatteri, M., and P. Spudich (2000), What can strong-motion data tell us about slip-weakening fault-friction laws?, *Bull. Seismol. Soc. Am.*, *90*(1), 98–116, doi:10.1785/0119990053.

Hamling, I. J., et al. (2017), Complex multi-fault rupture during the 2016 M_w 7.8 Kaikōura earthquake, New Zealand, *Science*, *356*(6334), doi:10.1126/science.aam7194.
Harris, R. A., et al. (2009), The SCEC/USGS dynamic earthquake rupture code verification exercise, *Seismol. Res. Lett.*, *80*(1), 119–126, doi:10.1785/gssrl.80.1.119.
Harris, R. A., et al. (2011), Verifying a computational method for predicting extreme ground motion, *Seismol. Res. Lett.*, *82*(5), 638–644, doi:10.1785/gssrl.82.5.638.
Heaton, T. H. (1990), Evidence for and implications of self-healing pulses of slip in earthquake rupture, *Phys. Earth Planet. Inter.*, *64*, 1–20.
Ida, Y. (1972), Cohesive force across the tip of a longitudinal-shear crack and Griffith's specific surface energy, *J. Geophys. Res.*, *77*, 3796–3805, doi:10.1029/JB077i020p03796.
Ide, S., and M. Takeo (1997), Determination of constitutive relations of fault slip based on seismic wave analysis, *J. Geophys. Res.*, *102*, 27,379–27,391.
Irikura, K., and H. Miyake (2011), Recipe for predicting strong ground motion from crustal earthquake scenarios, *Pure Appl. Geophys.*, *168*(1–2), 85–104.
Kaiser, A. E., C. V. Houtte, N. D. Perrin, L. Wotherspoon, and G. H. McVerry (2017a), Site characterisation of GeoNet stations for the 2016 strong motion database, *Bull. N. Z. Soc. Earthquake Eng.*, *50*(1), 39–49.
Kaiser, A. E., et al. (2017b), The Kaikōura (New Zealand) earthquake: Preliminary seismological report, *Seismol. Res. Lett.*, *88*(3), 1–13, doi:10.1785/0220170018.
Kanamori, H., and H. Heaton (2000), Microscopic and macroscopic physics of earthquakes, in *Geocomplexity and the Physics of Earthquakes, Geophys. Monogr. Ser.*, vol. 120, edited by J. B. Rundle, D. L. Turcotte, and W. Klein, pp. 147–163, AGU, Washington, D. C., doi:10.1029/GM120p0147.
Kaneko, Y., N. Lapusta, and J.-P. Ampuero (2008), Spectral element modeling of spontaneous earthquake rupture on rate and state faults: Effect of velocity-strengthening friction at shallow depths, *J. Geophys. Res.*, *113*, B09317, doi:10.1029/2007JB005553.
Kostrov, B. V. (1974), Seismic moment and energy of earthquakes and seismic flow of rock, *Izv., Acad. Sci., USSR, Phys. Solid Earth (Engl. Translation)*, *1*, 23–40.
Langridge, R. M., et al. (2016), The New Zealand active faults database, *N. Z. J. Geol. Geophys.*, *59*(1), 86–96.
Mikumo, T., K. B. Olsen, E. Fukuyama, and Y. Yagi (2003), Stress-breakdown time and slip-weakening distance inferred from slip-velocity functions on earthquake faults, *Bull. Seismol. Soc. Am.*, *93*(1), 264–282, doi:10.1785/0120020082.
Nielsen, S., E. Spagnuolo, S. Smith, M. Violay, G. D. Toro, and A. Bistacchi (2016), Scaling in natural and laboratory earthquakes, *Geophys. Res. Lett.*, *43*, 1504–1510, doi:10.1002/2015GL067490.
Noda, H., N. Lapusta, and H. Kanamori (2013), Comparison of average stress drop measures for ruptures with heterogeneous stress change and implications for earthquake physics, *Geophys. J. Int.*, *193*, 1691–1712, doi:10.1093/gji/ggt074.
Ohnaka, M. (2003), A constitutive scaling law and a unified comprehension for frictional slip failure, shear fracture of intact rock, and earthquake rupture, *J. Geophys. Res.*, *108*, 2080, doi:10.1029/2000JB000123.
Ohnaka, M., and L. F. Shen (1999), Scaling of the shear rupture process from nucleation to dynamic propagation: Implications of geometric irregularity of the rupturing surfaces, *J. Geophys. Res.*, *104*, 817–844, doi:10.1029/1998JB900007.
Ohnaka, M., Y. Kuwahara, and K. Yamamoto (1987), Constitutive relations between dynamic physical parameters near a tip of the propagating slip zone during stick-slip shear failure, *Tectonophysics*, *144*(1–3), 109–125.
Okada, Y. (1992), Internal deformation due to shear and tensile faults in a half-space, *Bull. Seismol. Soc. Am.*, *82*, 1018–1040.
Palmer, A. C., and J. R. Rice (1973), The growth of slip surfaces in the progressive failure of over-consolidated clay, *Proc. R. Soc. London, Ser. A*, *332*, 527–548.
Pulido, N., and K. Irikura (2000), Estimation of dynamic rupture parameters from the radiated seismic energy and apparent stress, *Geophys. Res. Lett.*, *27*(23), 3945–3948.
Rivera, L., and H. Kanamori (2005), Representations of the radiated energy in earthquakes, *Geophys. J. Int.*, *162*(1), 148–155.
Ruiz, S., and R. Madariaga (2011), Determination of the friction law parameters of the M_w 6.7 Michilla earthquake in northern Chile by dynamic inversion, *Geophys. Res. Lett.*, *38*, L09317, doi:10.1029/2011GL047147.
Tinti, E., P. Spudich, and M. Cocco (2005a), Earthquake fracture energy inferred from kinematic rupture models on extended faults, *J. Geophys. Res.*, *110*(B12303), doi:10.1029/2005JB003644.
Tinti, E., E. Fukuyama, A. Piatanesi, and M. Cocco (2005b), A kinematic source-time function compatible with earthquake dynamics, *Bull. Seismol. Soc. Am.*, *95*(4), 1211–1223.
Twardzik, C., S. Das, and R. Madariaga (2014), Inversion for the physical parameters that control the source dynamics of the 2004 Parkfield earthquake, *J. Geophys. Res. Solid Earth*, *119*, 7010–7027, doi:10.1002/2014JB011238.
Van Houtte, C., S. Bannister, C. Holden, S. Bourguignon, and G. McVerry (2017), The New Zealand strong motion database, *Bull. N. Z. Soc. Earthquake Eng.*, *50*(1), 1–20.
Viesca, R. C., and D. I. Garagash (2015), Ubiquitous weakening of faults due to thermal pressurization, *Nat. Geosci.*, *8*(11), 875–879, doi:10.1038/ngeo2554.
Wood, R. A., J. R. Pettinga, S. Bannister, G. Lamarche, and T. J. McMorran (1994), Structure of the Hanmer strike-slip basin, Hope fault, New Zealand, *Geol. Soc. Am. Bull.*, *106*(11), 1459–1473.
Ye, L., T. Lay, H. Kanamori, and L. Rivera (2016), Rupture characteristics of major and great ($M_w \geq 7.0$) megathrust earthquakes from 1990 to 2015: 1. Source parameter scaling relationships, *J. Geophys. Res. Solid Earth*, *121*, 845–863, doi:10.1002/2015JB012427.
Yeats, R. S., and K. R. Berryman (1987), South Island, New Zealand, and transverse ranges, California: A seismotectonic comparison, *Tectonics*, *6*(3), 363–376.